

Intratumor DNA Methylation Heterogeneity Reflects Clonal Evolution in Aggressive Prostate Cancer

David Brocks,¹ Yassen Assenov,¹ Sarah Minner,² Olga Bogatyrova,¹ Ronald Simon,² Christina Koop,² Christopher Oakes,¹ Manuela Zucknick,³ Daniel Bernhard Lipka,^{1,4} Joachim Weischenfeldt,⁵ Lars Feuerbach,⁶ Richard Cowper-Sal-lari,⁷ Mathieu Lupien,^{7,8,9} Benedikt Brors,⁶ Jan Korbel,^{5,10} Thorsten Schlomm,^{11,12} Amos Tanay,¹³ Guido Sauter,² Clarissa Gerhäuser,¹ Christoph Plass,^{1,14,*} and the ICGC Early Onset Prostate Cancer Project

¹Division of Epigenomics and Cancer Risk Factors, German Cancer Research Center, Im Neuenheimer Feld 280, 69120 Heidelberg, Germany

²Institute of Pathology, University Medical Center Hamburg-Eppendorf, Martinistraße 52, 20246 Hamburg, Germany

³Division of Biostatistics, German Cancer Research Center, Im Neuenheimer Feld 280, 69120 Heidelberg, Germany

⁴Department of Hematology and Oncology, University Medical Center, Otto-von-Guericke University, Leipziger Strasse 44, 39120 Magdeburg, Germany

⁵Genome Biology Unit, European Molecular Biology Laboratory (EMBL), Meyerhofstrasse 1, 69117 Heidelberg, Germany

⁶Division of Theoretical Bioinformatics, German Cancer Research Center, Im Neuenheimer Feld 280, 69120 Heidelberg, Germany

⁷The Princess Margaret Cancer Centre, University Health Network, 610 University Avenue, Toronto, ON M5G 1L7, Canada

⁸Ontario Institute for Cancer Research, 661 University Avenue, Toronto, ON M5G 0A3, Canada

⁹Department of Medical Biophysics, University of Toronto, TMDT, 101 College Street, Toronto, ON M5G 1L7, Canada

¹⁰European Bioinformatics Institute, Wellcome Trust Genome Campus, Hinxton, Cambridge CB10 1SD, UK

¹¹Martini-Clinic, Prostate Cancer Center, University Medical Center Hamburg-Eppendorf, Martinistraße 52, 20246 Hamburg, Germany

¹²Department of Urology, Section for Translational Prostate Cancer Research, University Medical Center Hamburg-Eppendorf, Martinistraße 52, 20246 Hamburg, Germany

¹³Department of Computer Science and Applied Mathematics and Department of Biological Regulation, Weizmann Institute of Science, Rehovot 76100, Israel

¹⁴The German Cancer Consortium, Im Neuenheimer Feld 280, 69120 Heidelberg, Germany

*Correspondence: c.plass@dkfz.de

<http://dx.doi.org/10.1016/j.celrep.2014.06.053>

This is an open access article under the CC BY-NC-ND license (<http://creativecommons.org/licenses/by-nc-nd/3.0/>).

SUMMARY

Despite much evidence on epigenetic abnormalities in cancer, it is currently unclear to what extent epigenetic alterations can be associated with tumors' clonal genetic origins. Here, we show that the prostate intratumor heterogeneity in DNA methylation and copy-number patterns can be explained by a unified evolutionary process. By assaying multiple topographically distinct tumor sites, premalignant lesions, and lymph node metastases within five cases of prostate cancer, we demonstrate that both DNA methylation and copy-number heterogeneity consistently reflect the life history of the tumors. Furthermore, we show cases of genetic or epigenetic convergent evolution and highlight the diversity in the evolutionary origins and aberration spectrum between tumor and metastatic subclones. Importantly, DNA methylation can complement genetic data by serving as a proxy for activity at regulatory domains, as we show through identification of high epigenetic heterogeneity at androgen-receptor-bound enhancers. Epigenome variation thereby expands on the current genome-centric view on tumor heterogeneity.

INTRODUCTION

Prostate adenocarcinoma is the most common cancer among men and globally causes over 250,000 deaths every year (Bray et al., 2013). Genetically, it is strongly dominated by copy-number and other structural alterations rather than by nonsynonymous point mutations (Baca et al., 2013; Barbieri et al., 2012; Berger et al., 2011; Grasso et al., 2012; Shen and Abate-Shen, 2010; Taylor et al., 2010; Weischenfeldt et al., 2013). Moreover, aberrant DNA methylation patterns are universally found in prostate tumors and are known to frequently affect genes involved in hormonal response, cell cycle control, and DNA damage repair (Börnö et al., 2012; Kobayashi et al., 2011; Li, 2007; Nelson et al., 2009). In light of the recent discoveries of extensive genetic intratumor heterogeneity (Almendro et al., 2014; Gerlinger et al., 2012; Johnson et al., 2014; Landau et al., 2013; Lohr et al., 2014; Navin et al., 2011; Navin, 2014; Nik-Zainal et al., 2012; Sottoriva et al., 2013), we analyzed how methylomes vary within the same prostate tumor and how such variation is associated with the diversity in genomic alterations and the evolutionary history of the tumor. Given that prostate cancers are dominated by structural alterations and that intratumor copy-number and mutational diversity are highly correlated during tumor evolution (Gerlinger et al., 2014), we focused on copy-number alterations as a measure of genomic intratumor variability. To simultaneously study methylome and copy-number patterns in multiple

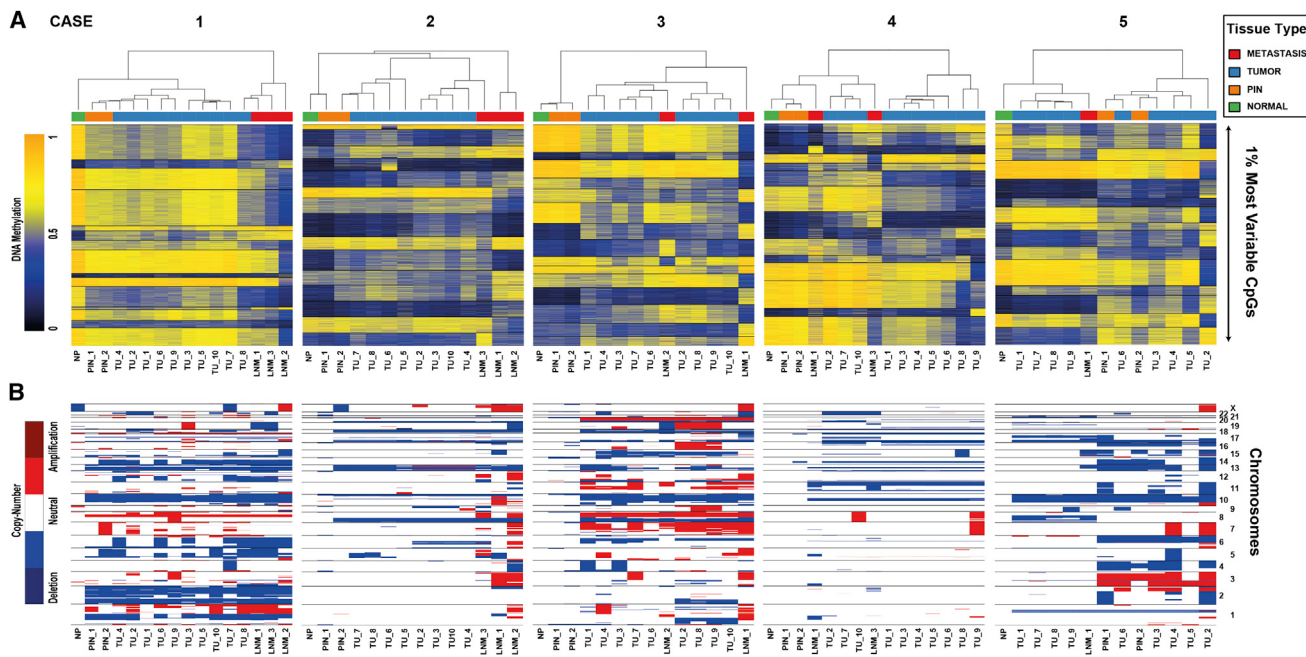


Figure 1. Subclonal Cell Populations Differ in Their Genetic and Epigenetic Profiles

(A) Unsupervised hierarchical clustering of intratumoral methylation patterns for cases 1–5 (left to right). Tissue types from each individual are color coded with green (normal [NP]), orange (premalignant lesions [PIN]), blue (primary tumor [TU]), and red (lymph node metastasis [LNM]). Rows of the heatmaps display the methylation levels of the patientwise top 1% CpG sites ($n = 4,457$) with the greatest intratumoral DNA methylation variability (range). Blue indicates low, and yellow represents high methylation level (from 0% to 100%).

(B) Copy-number alteration profiles from different regions of the same tumor (cases 1–5; left to right). Deletions (blue) and amplifications (red) are shown for chromosomes 1–X. Specimens are ordered according to the result of the unsupervised hierarchical cluster analysis of the methylation data (A).

spatially separated regions of a tumor, we used Illumina HumanMethylation450 BeadChip arrays, which not only target more than 450,000 CpG sites covering 99% of RefSeq genes but can also be employed to detect copy-number alterations with the sensitivity of SNP arrays (Feber et al., 2014; Oakes et al., 2014; Sturm et al., 2012). In total, the analyzed sample cohort consisted of multiple geographically distinct primary tumor sites (TU; $n = 10$), premalignant lesions (PIN; $n = 2$), lymph node metastases (LNM; $n = 3$), and matched normal prostate epithelium (NP; $n = 1$) from each five patients with aggressive prostate cancer (Table S1). Out of these in total 80 specimens, 72 were used for subsequent analyses; the others were excluded due to low tumor content or inconclusive copy-number profiles (Figure S1).

RESULTS

Extensive Genetic and Epigenetic Heterogeneity between Different Regions of the Same Tumor

We first performed unsupervised hierarchical clustering of both DNA methylation and copy-number patterns. This analysis showed that specimens of the same patient were generally more similar to each other than those from different individuals (Figures S2A and S2B), in line with the previously described interindividual heterogeneity of prostate cancer metastases (Aryee et al., 2013; Drake et al., 2013; Liu et al., 2009). In addition,

the presence of shared methylation patterns and chromosomal breakpoint profiles between all tumor regions of a patient indicated a monoclonal origin in all five cases. Analysis of intratumoral DNA methylation and copy-number patterns further demonstrated the presence of multiple subclonal cell populations that were characterized by both distinct copy-number as well as DNA methylation profiles (Figure 1). In contrast to copy-number gains and DNA hypomethylation, we found copy-number losses and DNA hypermethylation events to be more clonal, i.e., more frequently shared between tumor sites (Figures S2C and S2D). Genes affected by clonal deletions or hypermethylation events included known tumor suppressor genes, e.g., PTEN, TP53, or GSTP1, respectively (Figure S2E), suggesting that these alterations occurred earlier during prostate cancer pathogenesis. Of the 47 genes with ubiquitous promoter hypermethylation in all cases, 16 (34%) were associated with transcriptional repression in another cohort of prostate cancer (Figure S2F). Importantly, whereas events found across all tumor sites also appeared dominant in individual regions (Figure S2G), a dominant event in a single specimen did not necessarily predict presence across the entire tumor bulk (Figure S2H). Together, these data show the extensive spatial DNA methylation and copy-number heterogeneity in prostate cancers of a monoclonal origin and the utility of multiregion analysis for the identification of clonal DNA methylation alterations.

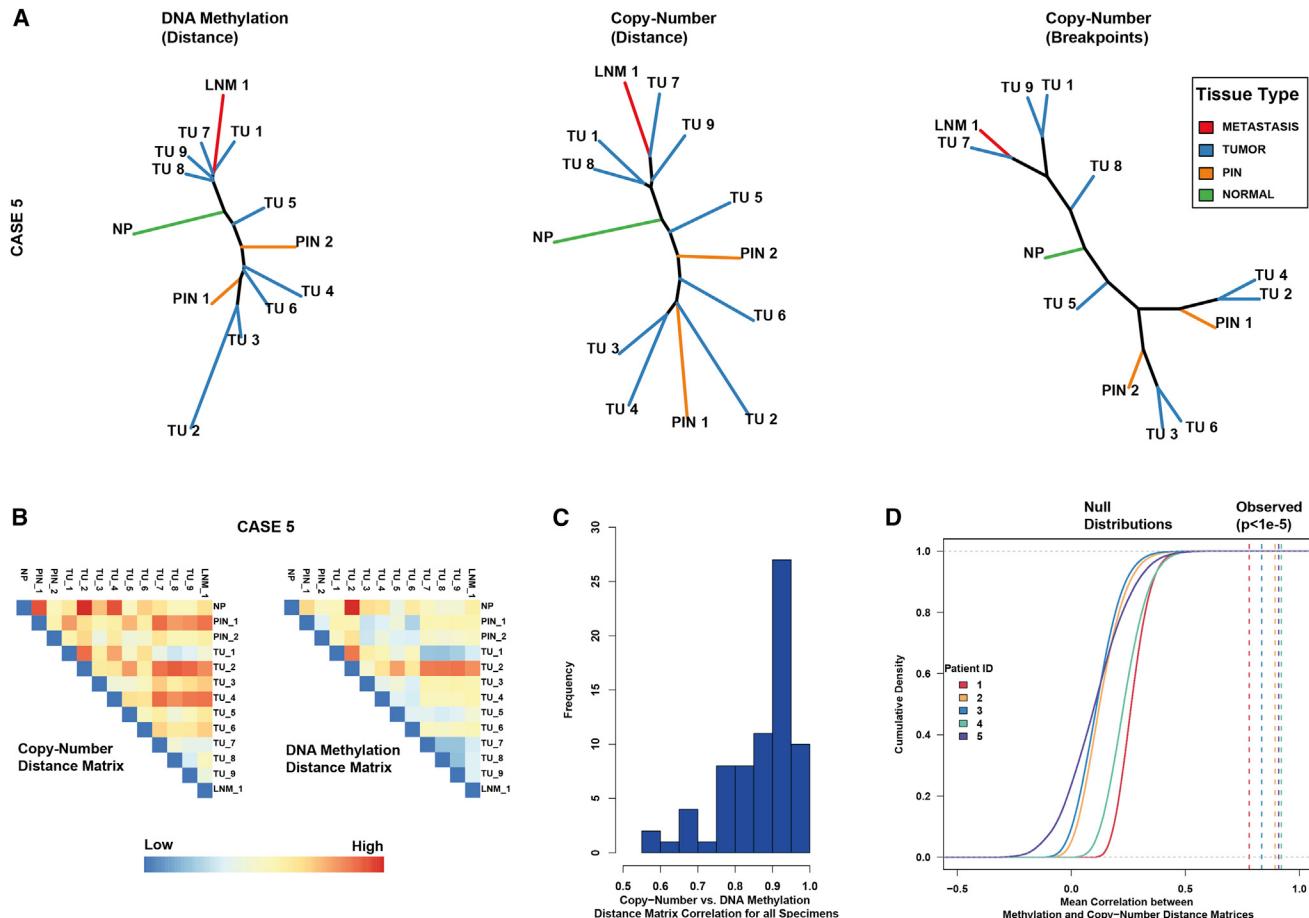


Figure 2. Unified Evolution of Methylation and Copy-Number Patterns

- (A) Phylogenetic reconstruction showing clonal relationships in case 5 inferred from DNA methylation (left), copy-number (center) distance matrices, or chromosomal breakpoint profiles (right). Tissue types are color coded with green (NP), orange (PIN), blue (TU), and red (LNM).
- (B) Illustration of genetic and epigenetic distance matrix comparison. Heatmaps show the Euclidean distance for all specimens of case 5 based on copy-number (left) and DNA methylation (right) patterns. Diagonal elements of the resulting correlation matrix were used to estimate the samplewise genetic and epigenetic correlation shown in (C). Colors represent Euclidean distance from low (blue) to high (red).
- (C) Distribution of the correlation between DNA methylation and copy-number distance matrices for all specimens.
- (D) Casewise mean correlation between genetic and epigenetic copy-number distance matrices (dotted lines) compared to the cumulative null distributions (sigmoidal curves) obtained by randomly permuting sample labels and repeating the steps 100,000 times. Color code indicates case number: one (red), two (yellow), three (blue), four (green), and five (purple).

Epigenetic Alterations Can Be Associated with the Clonal Architecture of Tumors

To study the association of genetic with epigenetic changes during tumor evolution, we inferred phylogenetic relationships based on either chromosomal breakpoint profiles (Letouzé et al., 2010) or based on pairwise distances of copy-number or methylation profiles as previously performed for copy-number or mutation data (Navin et al., 2011; Xu et al., 2012). DNA methylation and copy-number-derived phylogenetic tree topologies displayed high visual overlap (shown for case 5 in Figure 2A and for all others in Figure S3A). To better assess the similarity of intratumoral copy-number and DNA methylation patterns, we calculated the Pearson correlation coefficient between genetic and epigenetic distance matrices, which formed the basis of the inferred phylogenies (Figure 2B). Using this

approach for the five cases, we observed a strong linear relationship between genetic and epigenetic distances (median $R = 0.9$ of all 72 specimens; Figures 2C and S3B). Of note, we obtained consistent results also when using all CpGs, not only the most variable (median $R = 0.85$; Figure S3C), or after removal of all CpG sites within nondiploid copy-number regions (median $R = 0.84$; Figure S3D). We thus excluded that the high association between methylation and copy-number patterns is an artifact of a detection bias. To determine an empirical p value for the observed correlation, we compared the patient-wise mean correlation of genetic and epigenetic patterns against the null distributions obtained by randomly permuting sample labels. For all five cases, we found a highly significant association ($p < 1 \times 10^{-5}$; Figure 2D). Together, these data indicate that genome and epigenome diversity are not mutually

exclusive but can be explained by a unified evolutionary process.

Diversity in Metastatic Origin and Convergent Tumorigenic Processes

To further investigate the phylogenetic relationship of tumor subclones and to gain valuable clinical insight into the disease origin and progression for each of the five cases, we reconstructed consensus phylogenies based on both genetic and epigenetic data sets (Figure 3A). This combination gave more robust evolutionary models than the inferred clonal relationships based on genetic or epigenetic data sets alone (Figure S3E), displaying the utility of both measurements for distance-based evolutionary analyses. Consensus phylogenies demonstrated branched rather than linear evolutionary tumor growth, with clonal diversity not only within primary tumors but also between premalignant, primary, and metastatic sites. PIN lesions were either closely related to the normal prostate epithelium or diverged after the tumor bulk had already been established. Metastases originated from a shared subclonal ancestor (cases 1 and 2) or emerged independently from distinct tumor branches (cases 3 and 4). Critically, dissemination of metastasizing subclones was not always one of the latest events (like in case 1) but could occur earlier with respect to the emergence of the other primary tumor subpopulations (cases 2–5). Most noteworthy, the clone that gave rise to metastasis LNM_1 in case 4 lacked several of the chromosomal deletions otherwise found across all other tumor regions (Figure 1B), suggesting that the dissemination occurred before the two major tumor branches had evolved (Figure 3A). In addition, metastases always carried unique alterations not found in the primary tumor bulk and metastasis-specific aberrant methylation events frequently colocalized with genes involved in metastasis-associated processes, indicating that further genetic and epigenetic events were required for successful niche adaptation (Figure S4). Examination of phylogenetic relationships and underlying copy-number and DNA methylation profiles showed that phylogenetically distant tumor populations could independently acquire convergent copy-number states. For example, tumor subclonal cell populations TU_9 and TU_10 from case 4 autonomously gained large parts of chromosome 8 encoding the *MYC* oncogene (Figure 3B). Similarly, metastasis LNM_3 and primary tumors TU_8 and TU_9 (case 4) independently lost methylation at hundreds of corresponding CpG sites (Figure 3C) without any signs of convergent evolution at the copy-number level. Altogether, detailed reconstruction of genetic and epigenetic histories revealed independent and convergent tumorigenic evolutionary processes and facilitated identification of the evolutionary origins of metastases and tumor subpopulations.

Intratumor DNA Methylation Heterogeneity Predominantly Occurs at Prostate-Specific Gene Regulatory Elements

Given the extensive DNA methylation heterogeneity, we asked whether these variable patterns were equally distributed across the genome or were enriched at regions with potential functional relevance for prostate tumors. To address this question, we

examined the genomic context in which intratumoral heterogeneous CpG methylation most frequently occurred. Between normal prostate epithelia from the same or different individuals, DNA methylation variability was comparatively low and distributed homogeneously across the genome (Figure 4A). In contrast, enhancer sites exhibited substantial DNA methylation variability within tumors, whereas methylation at transcription start sites (TSS) and CpG islands (CGIs) remained relatively static during subclonal diversification. These observations are exemplified at the *MAPK3* locus, in which the regions with enhancer-associated chromatin marks displayed high DNA methylation variability whereas methylation at the TSS and CGIs remained relatively stable (Figure 4B). To characterize potential biological differences between static and variably methylated enhancer domains, we next examined the difference in transcription factor (TF) occupancy between these two groups. Five out of 65 TF motifs significantly enriched for variable over static enhancer domain binding ($p < 0.001$) showed enrichment in all five cases, including the androgen receptor (AR) response element and/or half-site-binding motif (Figure 4C). Consistently, enhancer domains bound by AR displayed significantly higher intratumoral methylation ranges compared to AR binding or enhancer regions alone (Figure 4D). Given the known importance of the AR in prostate tumorigenesis (Carver et al., 2011; Wang et al., 2009; Weischenfeldt et al., 2013; Yu et al., 2010), we further investigated the link between oncogenic TF binding and DNA methylation heterogeneity. Oncogenic TF binding was generally associated with low levels of DNA methylation across all tumor regions. However, AR-binding sites frequently deviated from that unmethylated state, whereas FOXA1- and especially ERG-binding sites remained more static (Figure 4E). These results demonstrate that the degree of intratumoral DNA methylation variability strongly depends on the genetic and epigenetic context of a locus. Furthermore, the preference of DNA methylation variability at prostate-specific gene-regulatory elements shows how methylome data might complement genetic information by serving as a proxy of regulatory activity in tumor subclones.

DISCUSSION

In this study, we have shown the profound genetic and epigenetic intratumor heterogeneity of advanced prostate cancer that also affected known prostate cancer drivers and genes of prognostic significance. Only a subset of aberrant DNA methylation events were recurrently found across all tumor regions, of which some coincided with transcriptional downregulation in prostate cancer. Regardless of whether these ubiquitous aberrant methylation events were already present in the most recent common ancestor or arose independently in distinct tumor subpopulations, our study suggests that the epigenome continues to evolve in parallel to the acquisition of driving and passenger copy-number mutations. Hence, we were able to associate epigenetic aberrations with the complex clonal genetic architecture of the tumors, confirming the view on somatic DNA methylation as a persistent rather than dynamically regulated modification (Shipony et al., 2014). This approach also allowed us to infer clonal relationships between

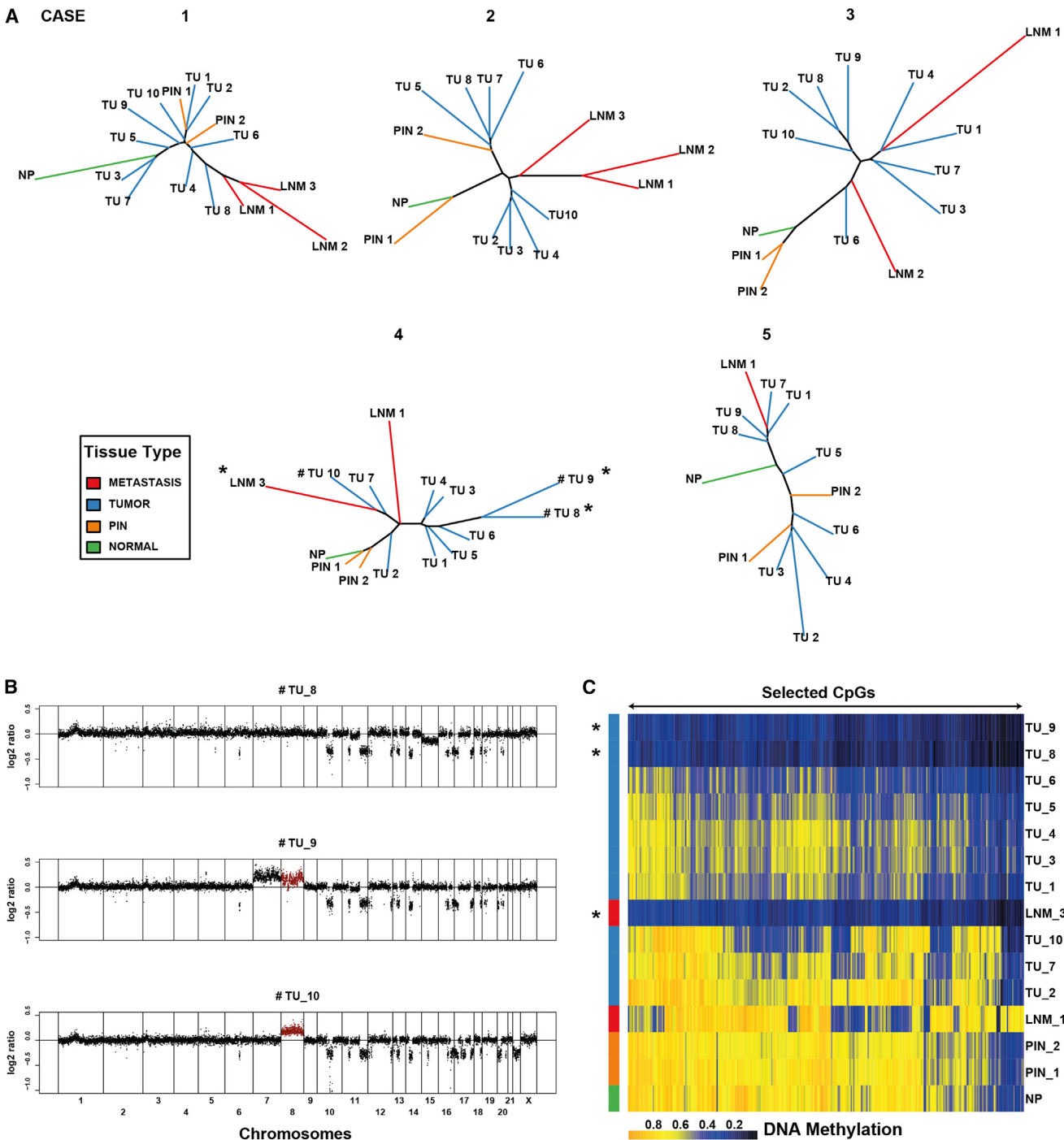


Figure 3. The Life History of Five Aggressive Prostate Cancers

(A) Consensus phylogenies based on merged genetic and epigenetic distance matrices for cases 1–5. Tissue types from each individual are color coded with green (NP), orange (PIN), blue (TU), and red (LNM). Copy-number profiles of specimens marked with a hash key are shown in (B) to illustrate convergent evolution of copy-number states. Specimens marked with an asterisk were used to illustrate convergent evolution of methylation patterns (C).

(B) Copy-number profiles of tumor samples TU_8, TU_9, and TU_10 from case 4 for chromosomes 1–X. Gained chromosome 8 in TU_9 and TU_10 is highlighted by red coloring.

(C) Convergent evolution of methylation patterns between metastasis 3 and tumor specimens 8 and 9 from case 4. Heatmap shows methylation of the CpG sites (304 out of the 4,557 most variable CpGs) with a significantly lower methylation level (Benjamini-Hochberg-adjusted p value < 0.01) in LNM_3, TU_8, and TU_9 compared to the other specimens. Blue indicates low, and yellow represents high methylation level (0%–100%). Specimens are arranged as in Figure 1. Tissue types are color coded with green (NP), orange (PIN), blue (TU), and red (LNM). Black asterisk denotes specimens with analogous methylation state.

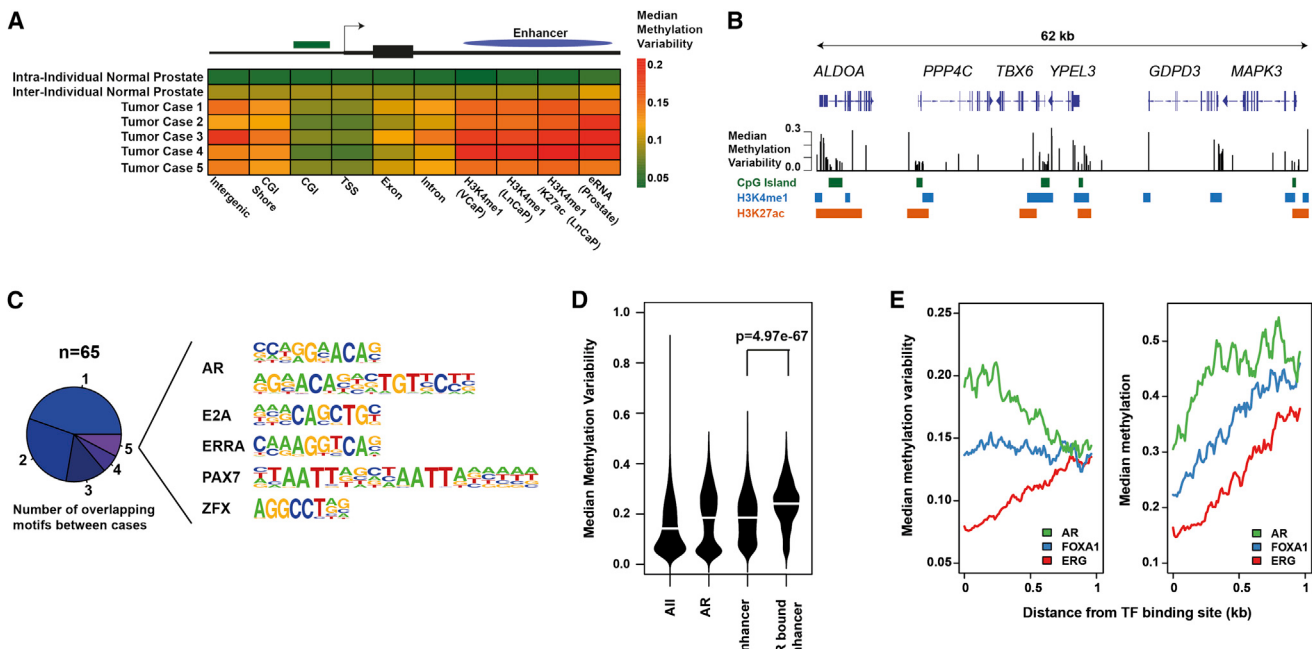


Figure 4. The Degree of Intratumoral Heterogeneous DNA Methylation Depends on the Genetic and Epigenetic Context of a Locus

(A) DNA methylation variability between normal prostate epithelia and within tumors 1–5. Intraindividual variability of normal prostates was assessed using specimens NP, PIN_1, and PIN_2 from case 3 whereas interindividual variability was analyzed by comparing normal prostates from the five cases. The median methylation variability (based on intraepithelial/tumoral range) of all analyzed CpG sites associated with indicated genomic contexts is shown by colors ranging from green (0.05) to red (0.2). Enhancers were defined by chromatin immunoprecipitation sequencing signals of predictive chromatin marks (H3K27ac and/or H3K4me1) or enhancer RNAs of the normal prostate gland. CGI, CpG islands; eRNA, enhancer RNA; TSS, transcription start site.

(B) Median intratumoral DNA methylation variability (based on intratumoral range) between prostate cancer cases 1–5 for all analyzed CpG sites in a 62 kb region including the *MAPK3* gene locus. Green track denotes CpG islands, blue track indicates H3K4me1 peaks, and orange track displays H3K27ac domains.

(C) Transcription-factor-binding motifs ($n = 65$) showing significant ($p < 0.001$) enrichment for binding at variably methylated enhancer domains. Pie chart indicates the number of cases a TF motif was found to be significantly enriched in. Enrichment in all five cases was observed for androgen receptor (AR), E2A immunoglobulin-enhancer-binding factors E12/E47 (E2A), estrogen-related receptor alpha (ERRα), paired box protein 7 (PAX7), and zinc finger X-chromosomal protein (ZFX).

(D) Intratumoral DNA methylation variability of all CpGs or CpG sites colocalizing with AR-binding sites, enhancer domains (H3K4me1), or both. Width of the beanplot indicates CpG density, and white lines show median methylation variability (range). Differences between enhancer and AR-bound enhancer are statistically significant (Wilcoxon test; $p = 4.97 \times 10^{-67}$).

(E) Median methylation variability (left) and median methylation levels (right) as a function of distance to AR- (green), FOXA1- (blue), or ERG- (red) binding sites in LNCaP prostate cancer cells.

primary tumor and metastatic subclones, which revealed the broad diversity in metastatic origin and the associated genetic and epigenetic alterations. Future studies applying multiregion analysis on hundreds of different tumors and corresponding metastases will allow generalization about how frequently the described evolutionary patterns actually occur in patients. In addition to providing information on the genetic clonal relationships, DNA methylation adds information about regulatory activity at important cis-regulatory elements (Feldmann et al., 2013; Stadler et al., 2011), as we have demonstrated by cases of convergent and metastasis-specific aberrant methylation, as well as through identification of high epigenetic heterogeneity at androgen-receptor-bound enhancer domains. Consequently, deducing tumor evolution that is based on epigenomic data does not only allow rapid and sensitive reconstruction of tumor structure but could potentially provide information on the functional state of tumor subclones and thereby assist in future clinical decision making.

EXPERIMENTAL PROCEDURES

Patient Material

Research using pseudomized human leftover tissue samples from routine diagnosis is covered by the Hamburgisches Krankenhausgesetz (HmbKG) §12. The study protocol (PV3552) was approved by the Institutional Review Board of the Aerztekammer Hamburg (Chair: Prof. T. Weber). Informed consent was obtained from all subjects involved in this study. A total of five prostate cancer patients were selected that had large unifocal prostate cancers, adjacent high-grade PIN that was large enough to be separately analyzed, and at least three nodal metastases measuring ≥ 1 cm. All prostates from these patients had been prepared according to standard protocols (Erbersdobler et al., 2002), including complete paraffin embedding of the entire prostates. For selection of tumor regions, estimation of tumor cellularity, and nucleic acid isolation, see the [Supplemental Experimental Procedures](#).

DNA Methylation Profiling

Genome-wide DNA methylation was analyzed on Illumina HumanMethylation450 BeadChip arrays (Illumina). Methylation of tumor and normal prostate

samples was measured according to the manufacturer's instruction at the DKFZ Genomics and Proteomics Core Facility. Data were analyzed using the RnBeads pipeline (<http://rnbeads.mpi-inf.mpg.de/>) as described in the *Supplemental Experimental Procedures*.

Copy-Number Alterations Profiling

Copy-number alterations (CNAs) were interrogated from the Illumina Human-Methylation450 BeadChip with the sum of the methylated and unmethylated signal intensities (Sturm et al., 2012) as described in the *Supplemental Experimental Procedures*.

Unsupervised Hierarchical Clustering

For hierarchical clustering of casewise intratumoral methylation levels, a Euclidean distance calculation and Ward's linkage was performed for the top 1% of probes with the greatest difference between intratumoral maximal and minimal methylation (range). Normal epithelia and normal-like PIN lesions (2_PIN_1, 3_PIN_1, 3_PIN_2, 4_PIN_1, and 4_PIN_2) were excluded for the calculation of intratumoral DNA methylation range.

Phylogenetic Reconstruction

Top 1% (n = 4,457) of CpG sites with the greatest intratumoral methylation range were used to generate DNA methylation Euclidean distance matrices. For the calculation of intratumoral DNA methylation range, normal epithelia and normal-like PIN lesions (2_PIN_1, 3_PIN_1, 3_PIN_2, 4_PIN_1, and 4_PIN_2) were excluded. Methylation-based phylogenetic trees were inferred by the minimal evolution method (Desper and Gascuel, 2002) using the fastme.bal function in the R package ape. CNA-based phylogenies were either generated using TuMult (Letouzé et al., 2010; parameters th.bkp = 2) or by applying the minimal evolution algorithm on CNA Euclidean distance matrices that were based on continuous log2 ratios of the intensities. For consensus phylogenetic reconstruction, CNA and methylation distance matrices were elementwise added after being divided by their medians and clonal relationships were inferred by applying the minimal evolution algorithm on the merged CNA and methylation distance matrices. Strength of support for clades on phylogenetic trees was assessed by bootstrapping (1,000 bootstrap replicates) using the boot.phylo function from the R package ape.

Correlation between Copy-Number Alteration and Methylation Distances

Casewise Euclidean distance matrices were generated based on continuous CNA log2 ratios of the intensities or the top 1% DNA methylation probes with the highest casewise intratumoral variability (range), unless otherwise stated. For the calculation of intratumoral DNA methylation range, normal epithelia and normal-like PIN lesions (2_PIN_1, 3_PIN_1, 3_PIN_2, 4_PIN_1, and 4_PIN_2) were excluded. Similarity was assessed by calculating the Pearson's correlation coefficient between the genetic and epigenetic distance matrices. Samplewise correlation was obtained by using the diagonal elements of the resulting correlation matrix. An empirical p value was generated by comparing the mean of the correlation matrix diagonal elements to a null distribution generated by permuting sample labels and repeating the steps 100,000 times.

Genomic Context

Exon, intron, and TSS coordinates for RefSeq genes were downloaded from University of California, Santa Cruz. Promoters were defined as 1.5 kb upstream and 0.5 kb downstream of RefSeq TSS. CpG islands and shores were defined by standard Illumina 450K annotation. Previously reported (Yu et al., 2010) AR, ERG, FOXA1, and H3K4me1 peaks from LNCaP (H3K4me1 also VCaP) prostate cancer cells as well as LNCaP H3K27ac peaks (Hazelett et al., 2014) were downloaded from (<http://www.cistrome.org>). Enhancers of the primary prostate gland, defined by differential enhancer RNA expression (Andersson et al., 2014), were downloaded from (http://enhancer.binf.ku.dk/Pre-defined_tracks.html).

Motif Enrichment

Transcription factor motif enrichment was calculated using the Homer software package (Heinz et al., 2010). CpGs colocalizing with H3K4me1

peaks were extended by 100 bp in both directions. Motif enrichment for variably methylated (above median methylation variability at H3K4me1 peaks) enhancer CpGs was calculated in the resulting 200 bp regions against the statically methylated (below median methylation variability at H3K4me1 peaks) CpG 200 bp regions using the CpG-normalization option.

ACCESSION NUMBERS

The European Genome-Phenome Archive (<https://www.ebi.ac.uk/ega/>) accession number for the Illumina 450K arrays reported in this paper is EGAS00001000682.

SUPPLEMENTAL INFORMATION

Supplemental Information includes Supplemental Experimental Procedures, four figures, and one table and can be found with this article online at <http://dx.doi.org/10.1016/j.celrep.2014.06.053>.

AUTHOR CONTRIBUTIONS

D.B. performed data analysis and wrote the manuscript with the help of C.P. Y.A. was responsible for primary data quality control and statistical assistance. S.M., R.S., C.K., and T.S. conducted pathological assessments. L.F. estimated tumor cellularity. B.B., J.W., J.K., C.O., and M.Z. provided statistical assistance. O.B. isolated nucleic acids and was involved in phylogenetic reconstruction. D.B.L. performed motif-enrichment analysis. R.C.-S. and M.L. called chromatin states in LNCaP prostate cancer cell lines. C.P., G.S., C.G., and A.T. conceived and supervised the study.

ACKNOWLEDGMENTS

We thank the C.P. laboratory, M. Pudenz, K. Heilmann, M. Weiss, V. Hovestadt, E. Letouze, S. Haas, M. Milsom, and D. Weichenhan for feedback and discussions. D.B. is supported by the German-Israeli Helmholtz Research School in Cancer Biology. The authors acknowledge assistance from the DKFZ Genomics and Proteomics Core Facility. We also thank Pavel Komardin for help with data upload and Mor Moria-Shipony for designing the graphical abstract. This work was supported in part by the Helmholtz Association and the German Federal Ministry of Education and Science in the program for medical genome research (FKZ: 01KU1001A).

Received: March 18, 2014

Revised: May 9, 2014

Accepted: June 25, 2014

Published: July 24, 2014

REFERENCES

- Almendro, V., Cheng, Y.K., Randles, A., Itzkovitz, S., Marusyk, A., Ametller, E., Gonzalez-Farre, X., Muñoz, M., Russnes, H.G., Helland, A., et al. (2014). Inference of tumor evolution during chemotherapy by computational modeling and *in situ* analysis of genetic and phenotypic cellular diversity. *Cell Reports* 6, 514–527.
- Andersson, R., Gebhard, C., Miguel-Escalada, I., Hoof, I., Bornholdt, J., Boyd, M., Chen, Y., Zhao, X., Schmidl, C., Suzuki, T., et al.; FANTOM Consortium (2014). An atlas of active enhancers across human cell types and tissues. *Nature* 507, 455–461.
- Aryee, M.J., Liu, W., Engelmann, J.C., Nuhn, P., Gurel, M., Haffner, M.C., Esopi, D., Irizarry, R.A., Getzenberg, R.H., Nelson, W.G., et al. (2013). DNA methylation alterations exhibit intraindividual stability and interindividual heterogeneity in prostate cancer metastases. *Sci. Transl. Med.* 5, 69ra10.
- Baca, S.C., Prandi, D., Lawrence, M.S., Mosquera, J.M., Romanel, A., Drier, Y., Park, K., Kitabayashi, N., MacDonald, T.Y., Ghandi, M., et al. (2013). Punctuated evolution of prostate cancer genomes. *Cell* 153, 666–677.

- Barbieri, C.E., Baca, S.C., Lawrence, M.S., Demichelis, F., Blattner, M., Theurillat, J.P., White, T.A., Stojanov, P., Van Allen, E., Stransky, N., et al. (2012). Exome sequencing identifies recurrent SPOP, FOXA1 and MED12 mutations in prostate cancer. *Nat. Genet.* 44, 685–689.
- Berger, M.F., Lawrence, M.S., Demichelis, F., Drier, Y., Cibulskis, K., Sivachenko, A.Y., Sboner, A., Esgueva, R., Pflueger, D., Sougnez, C., et al. (2011). The genomic complexity of primary human prostate cancer. *Nature* 470, 214–220.
- Börnö, S.T., Fischer, A., Kerick, M., Fältth, M., Laible, M., Bräse, J.C., Kuner, R., Dahl, A., Grimm, C., Sayanjanli, B., et al. (2012). Genome-wide DNA methylation events in TMPRSS2-ERG fusion-negative prostate cancers implicate an EZH2-dependent mechanism with miR-26a hypermethylation. *Cancer Discov* 2, 1024–1035.
- Bray, F., Ren, J.S., Masuyer, E., and Ferlay, J. (2013). Global estimates of cancer prevalence for 27 sites in the adult population in 2008. *Int. J. Cancer* 132, 1133–1145.
- Carver, B.S., Chapinski, C., Wongvipat, J., Hieronymus, H., Chen, Y., Chandarlapaty, S., Arora, V.K., Le, C., Koutcher, J., Scher, H., et al. (2011). Reciprocal feedback regulation of PI3K and androgen receptor signaling in PTEN-deficient prostate cancer. *Cancer Cell* 19, 575–586.
- Desper, R., and Gascuel, O. (2002). Fast and accurate phylogeny reconstruction algorithms based on the minimum-evolution principle. *J. Comput. Biol.* 9, 687–705.
- Drake, J.M., Graham, N.A., Lee, J.K., Stoyanova, T., Faltermeier, C.M., Sud, S., Titz, B., Huang, J., Pienta, K.J., Graeber, T.G., and Witte, O.N. (2013). Metastatic castration-resistant prostate cancer reveals intrapatient similarity and interpatient heterogeneity of therapeutic kinase targets. *Proc. Natl. Acad. Sci. USA* 110, E4762–E4769.
- Erbersdobler, A., Fritz, H., Schnöger, S., Graefen, M., Hammerer, P., Huland, H., and Henke, R.P. (2002). Tumour grade, proliferation, apoptosis, micro-vessel density, p53, and bcl-2 in prostate cancers: differences between tumours located in the transition zone and in the peripheral zone. *Eur. Urol.* 41, 40–46.
- Feber, A., Guilhamon, P., Lechner, M., Fenton, T., Wilson, G.A., Thirlwell, C., Morris, T.J., Flanagan, A.M., Teschendorff, A.E., Kelly, J.D., and Beck, S. (2014). Using high-density DNA methylation arrays to profile copy number alterations. *Genome Biol.* 15, R30.
- Feldmann, A., Ivanek, R., Murr, R., Gaidatzis, D., Burger, L., and Schübeler, D. (2013). Transcription factor occupancy can mediate active turnover of DNA methylation at regulatory regions. *PLoS Genet.* 9, e1003994.
- Gerlinger, M., Rowan, A.J., Horswell, S., Larkin, J., Endesfelder, D., Gronroos, E., Martinez, P., Matthews, N., Stewart, A., Tarpey, P., et al. (2012). Intratumor heterogeneity and branched evolution revealed by multiregion sequencing. *N. Engl. J. Med.* 366, 883–892.
- Gerlinger, M., Horswell, S., Larkin, J., Rowan, A.J., Salm, M.P., Varela, I., Fisher, R., McGranahan, N., Matthews, N., Santos, C.R., et al. (2014). Genomic architecture and evolution of clear cell renal cell carcinomas defined by multiregion sequencing. *Nat. Genet.* 46, 225–233.
- Grasso, C.S., Wu, Y.M., Robinson, D.R., Cao, X., Dhanasekaran, S.M., Khan, A.P., Quist, M.J., Jing, X., Lonigro, R.J., Brenner, J.C., et al. (2012). The mutational landscape of lethal castration-resistant prostate cancer. *Nature* 487, 239–243.
- Hazelett, D.J., Rhie, S.K., Gaddis, M., Yan, C., Lakeland, D.L., Coetzee, S.G., Henderson, B.E., Noushmehr, H., Cozen, W., Kote-Jarai, Z., et al.; Ellipse/GAME-ON consortium; Practical consortium (2014). Comprehensive functional annotation of 77 prostate cancer risk loci. *PLoS Genet.* 10, e1004102.
- Heinz, S., Benner, C., Spann, N., Bertolino, E., Lin, Y.C., Laslo, P., Cheng, J.X., Murre, C., Singh, H., and Glass, C.K. (2010). Simple combinations of lineage-determining transcription factors prime cis-regulatory elements required for macrophage and B cell identities. *Mol. Cell* 38, 576–589.
- Johnson, B.E., Mazor, T., Hong, C., Barnes, M., Aihara, K., McLean, C.Y., Fouse, S.D., Yamamoto, S., Ueda, H., Tatsuno, K., et al. (2014). Mutational analysis reveals the origin and therapy-driven evolution of recurrent glioma. *Science* 343, 189–193.
- Kobayashi, Y., Absher, D.M., Gulzar, Z.G., Young, S.R., McKenney, J.K., Peehl, D.M., Brooks, J.D., Myers, R.M., and Sherlock, G. (2011). DNA methylation profiling reveals novel biomarkers and important roles for DNA methyltransferases in prostate cancer. *Genome Res.* 21, 1017–1027.
- Landau, D.A., Carter, S.L., Stojanov, P., McKenna, A., Stevenson, K., Lawrence, M.S., Sougnez, C., Stewart, C., Sivachenko, A., Wang, L., et al. (2013). Evolution and impact of subclonal mutations in chronic lymphocytic leukemia. *Cell* 152, 714–726.
- Letouzé, E., Allory, Y., Bollet, M.A., Radvanyi, F., and Guyon, F. (2010). Analysis of the copy number profiles of several tumor samples from the same patient reveals the successive steps in tumorigenesis. *Genome Biol.* 11, R76.
- Li, L.C. (2007). Epigenetics of prostate cancer. *Front. Biosci.* 12, 3377–3397.
- Liu, W., Laitinen, S., Khan, S., Viñinen, M., Kowalski, J., Yu, G., Chen, L., Ewing, C.M., Eisenberger, M.A., Carducci, M.A., et al. (2009). Copy number analysis indicates monoclonal origin of lethal metastatic prostate cancer. *Nat. Med.* 15, 559–565.
- Lohr, J.G., Stojanov, P., Carter, S.L., Cruz-Gordillo, P., Lawrence, M.S., Auclair, D., Sougnez, C., Knobochel, B., Gould, J., Saksena, G., et al.; Multiple Myeloma Research Consortium (2014). Widespread genetic heterogeneity in multiple myeloma: implications for targeted therapy. *Cancer Cell* 25, 91–101.
- Navin, N.E. (2014). Tumor evolution in response to chemotherapy: phenotype versus genotype. *Cell Reports* 6, 417–419.
- Navin, N., Kendall, J., Troge, J., Andrews, P., Rodgers, L., McIndoo, J., Cook, K., Stepansky, A., Levy, D., Esposito, D., et al. (2011). Tumour evolution inferred by single-cell sequencing. *Nature* 472, 90–94.
- Nelson, W.G., De Marzo, A.M., and Yegnasubramanian, S. (2009). Epigenetic alterations in human prostate cancers. *Endocrinology* 150, 3991–4002.
- Nik-Zainal, S., Van Loo, P., Wedge, D.C., Alexandrov, L.B., Greenman, C.D., Lau, K.W., Raine, K., Jones, D., Marshall, J., Ramakrishna, M., et al.; Breast Cancer Working Group of the International Cancer Genome Consortium (2012). The life history of 21 breast cancers. *Cell* 149, 994–1007.
- Oakes, C.C., Claus, R., Gu, L., Assenov, Y., Hullein, J., Zucknick, M., Bieg, M., Brocks, D., Bogatyrova, O., Schmidt, C.R., et al. (2014). Evolution of DNA methylation is linked to genetic aberrations in chronic lymphocytic leukemia. *Cancer Discov.* 4, 348–361.
- Shen, M.M., and Abate-Shen, C. (2010). Molecular genetics of prostate cancer: new prospects for old challenges. *Genes Dev.* 24, 1967–2000.
- Shipony, Z., Mukamel, Z., Mendelson Cohen, N., Landan, G., Chomsky, E., Reich Zeliger, S., Chagit Fried, Y., Ainbinder, E., Friedman, N., and Tanay, A. (2014). Dynamic and stable maintenance of epigenetic memory in pluripotent and somatic cells. *Nature* Published online July 13, 2014. <http://dx.doi.org/10.1038/nature13458>.
- Sottoriva, A., Spiteri, I., Piccirillo, S.G., Touloumis, A., Collins, V.P., Marioni, J.C., Curtis, C., Watts, C., and Tavaré, S. (2013). Intratumor heterogeneity in human glioblastoma reflects cancer evolutionary dynamics. *Proc. Natl. Acad. Sci. USA* 110, 4009–4014.
- Stadler, M.B., Murr, R., Burger, L., Ivanek, R., Liener, F., Schöler, A., van Nimwegen, E., Wirbelauer, C., Oakeley, E.J., Gaidatzis, D., et al. (2011). DNA-binding factors shape the mouse methylome at distal regulatory regions. *Nature* 480, 490–495.
- Sturm, D., Witt, H., Hovestadt, V., Khuong-Quang, D.A., Jones, D.T., Konermann, C., Pfaff, E., Tönjes, M., Sill, M., Bender, S., et al. (2012). Hotspot mutations in H3F3A and IDH1 define distinct epigenetic and biological subgroups of glioblastoma. *Cancer Cell* 22, 425–437.
- Taylor, B.S., Schultz, N., Hieronymus, H., Gopalan, A., Xiao, Y., Carver, B.S., Arora, V.K., Kaushik, P., Cerami, E., Reva, B., et al. (2010). Integrative genomic profiling of human prostate cancer. *Cancer Cell* 18, 11–22.

- Wang, Q., Li, W., Zhang, Y., Yuan, X., Xu, K., Yu, J., Chen, Z., Beroukhim, R., Wang, H., Lupien, M., et al. (2009). Androgen receptor regulates a distinct transcription program in androgen-independent prostate cancer. *Cell* 138, 245–256.
- Weischenfeldt, J., Simon, R., Feuerbach, L., Schlangen, K., Weichenhan, D., Minner, S., Wuttig, D., Warnatz, H.J., Stehr, H., Rausch, T., et al. (2013). Integrative genomic analyses reveal an androgen-driven somatic alteration landscape in early-onset prostate cancer. *Cancer Cell* 23, 159–170.
- Xu, X., Hou, Y., Yin, X., Bao, L., Tang, A., Song, L., Li, F., Tsang, S., Wu, K., Wu, H., et al. (2012). Single-cell exome sequencing reveals single-nucleotide mutation characteristics of a kidney tumor. *Cell* 148, 886–895.
- Yu, J., Yu, J., Mani, R.S., Cao, Q., Brenner, C.J., Cao, X., Wang, X., Wu, L., Li, J., Hu, M., et al. (2010). An integrated network of androgen receptor, polycomb, and TMPRSS2-ERG gene fusions in prostate cancer progression. *Cancer Cell* 17, 443–454.

Cell Reports, Volume 8

Supplemental Information

Intratumor DNA Methylation Heterogeneity Reflects Clonal Evolution in Aggressive Prostate Cancer

**David Brocks, Yassen Assenov, Sarah Minner, Olga Bogatyrova, Ronald Simon,
Christina Koop, Christopher Oakes, Manuela Zucknick, Daniel Bernhard Lipka,
Joachim Weischenfeldt, Lars Feuerbach, Richard Cowper-Sal-lari, Mathieu Lupien,
Benedikt Brors, Jan Korbel, Thorsten Schlomm, Amos Tanay, Guido Sauter, Clarissa
Gerhäuser, and Christoph Plass**

Table S1, related to experimental procedures. Clinical characteristics of the analyzed prostate adenocarcinomas

Case-ID.	Patient age	Tumor stage	Gleason	Nodal stage	Positive lymph nodes/total of lymph nodes examined
1	50	pT3b	4+5=9	pN1	5/25
2	61	pT3b	4+5=9	pN1	6/18
3	53	pT3b	4+5=9	pN1	7/31
4	57	pT3b	4+3=7, tertiary grade 5	pN1	6/16
5	62	pT3b	3+4=7, tertiary grade 5	pN1	4/14

Figure S1

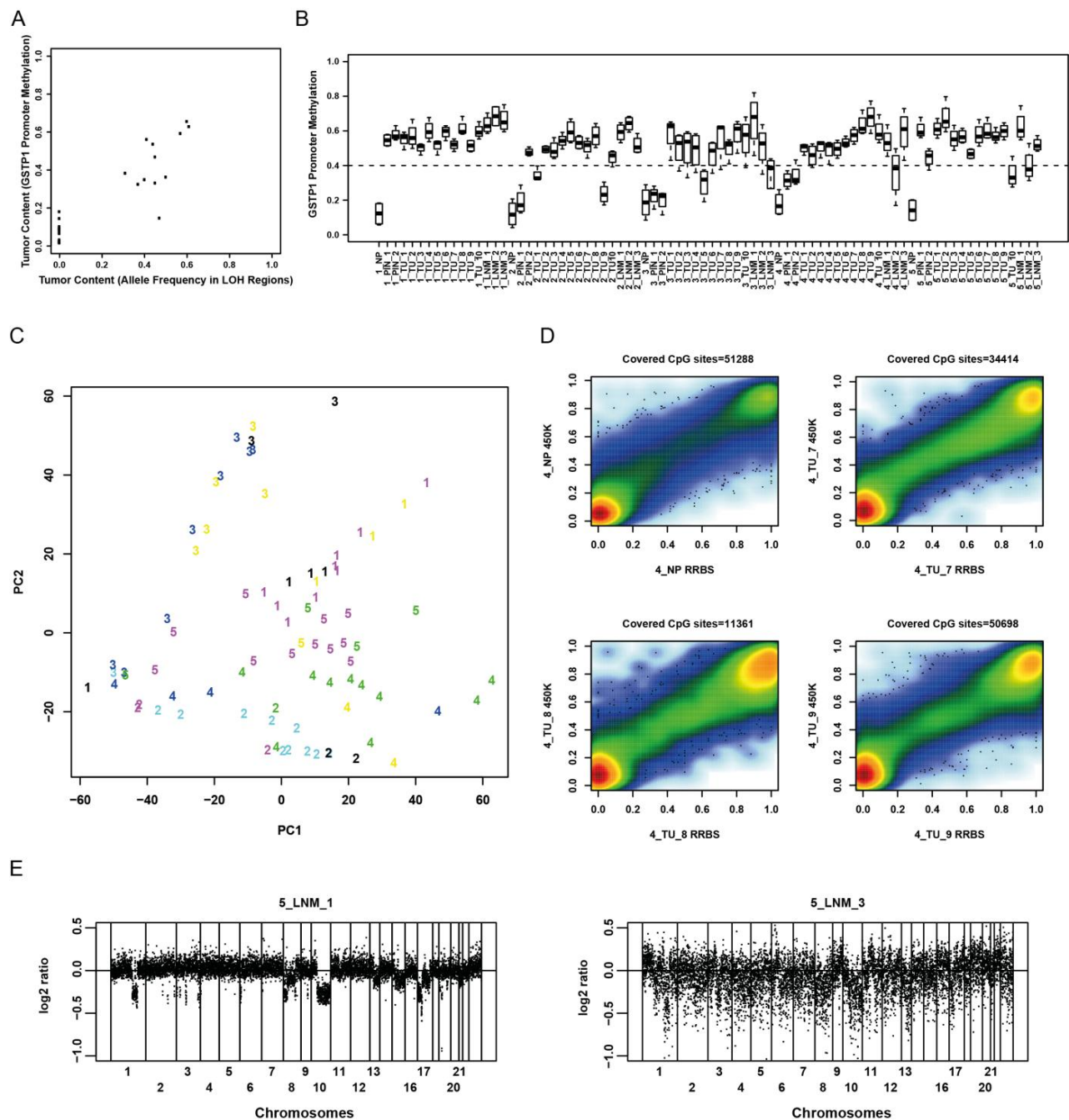


Figure S1, related to experimental procedures. Quality control of tumor samples and Illumina 450K data.

- A) Tumor content estimation based on GSTP1 promoter methylation and allele frequency of germline SNVs in LOH regions in a different cohort of prostate cancer samples ($R=0.9$).
- B) Boxplot of GSTP1 promoter methylation (beta value) for all samples. Non-PIN specimens having a median (black lines) methylation below 0.4 (vertical dotted line) were excluded from the analysis; 2_TU_1, 2_TU_9, 3_TU_5, 3_LNM_3, 4_LNM_2, 5_TU_10, and 5_LNM_2. PIN-lesions below 0.4 were kept for analysis. Retained specimens varied in purity between 45 % and 70 % of tumor content which was better or comparable to other studies that have assessed tumor content by sequencing based methods (Baca et al., 2013; Su et al., 2012).
- C) Principle component analysis of methylation values. Numbers and color indicate case ID and Sentrix ID, respectively.
- D) Comparison of methylation levels measured by Illumina 450K against reduced-representation bisulfite-sequencing (RRBS). Color indicates density from lightblue (low) to red (high). The observed Pearson correlation between 450K and RRBS data for samples 4_NP, 4_TU_7, 4_TU_8, and 4_TU_9 was 0.954, 0.959, 0.96, and 0.96, respectively.
- E) Copy-number alteration profiles based on the sum of methylated and unmethylated signal intensities. Left profile (5_LNM_1) shows a representative copy-number alterations profile from chromosome 1 to X that was inferred from 450K signal intensities. Right profile (5_LNM_3) was excluded from the analysis due to high signal noise.

Figure S2

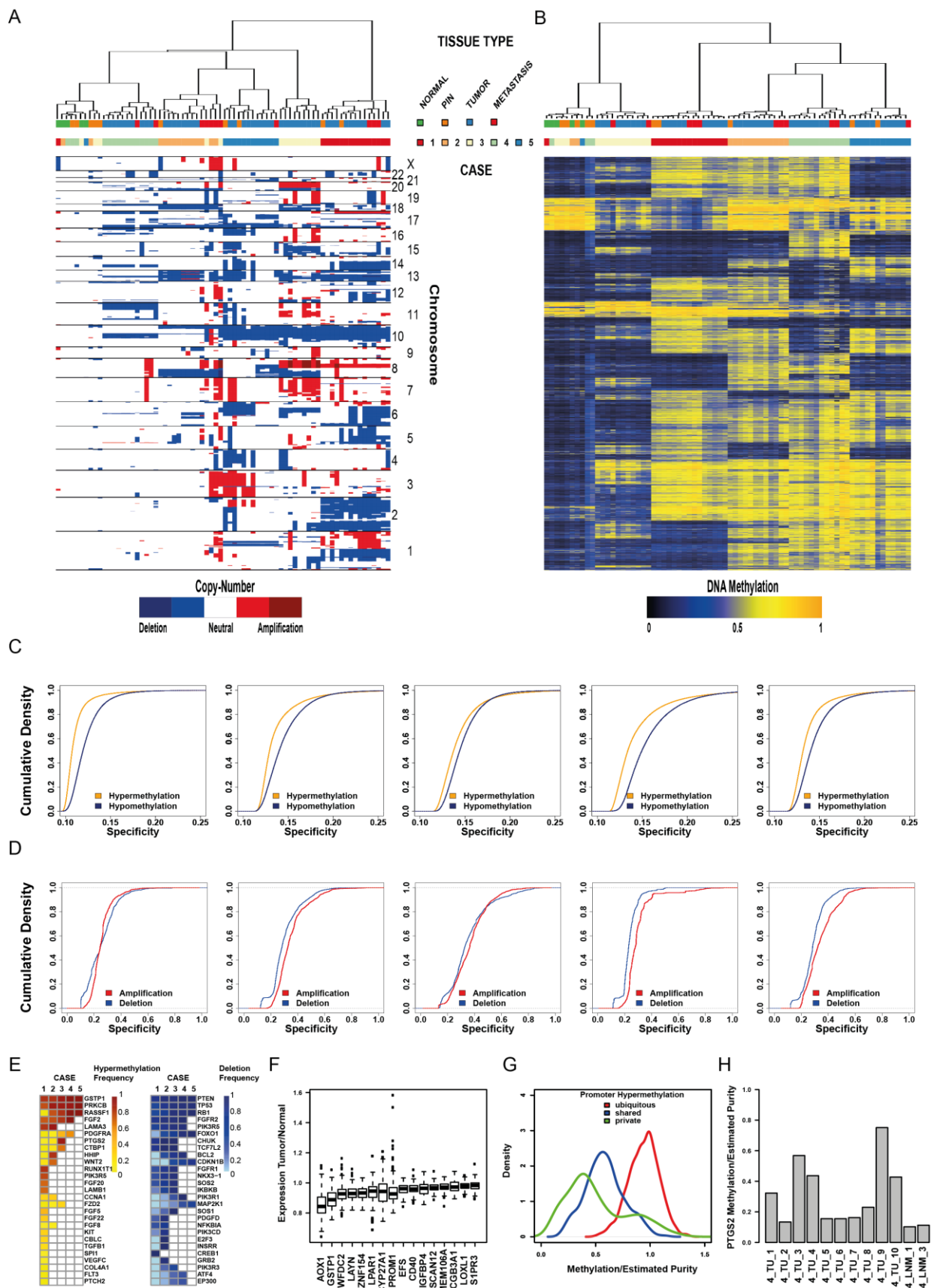


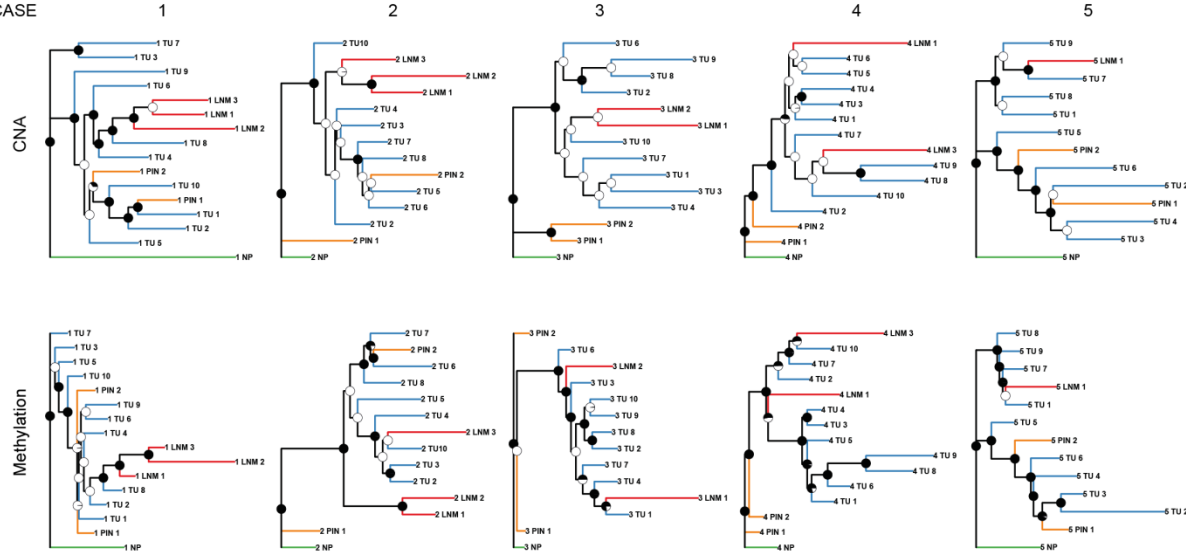
Figure S2, related to Figure 1. Frequency of genetic and epigenetic aberrations across different tumor regions.

- A) Unsupervised hierarchical clustering of intertumoral copy-number profiles from five cases with aggressive prostate cancer (1-5; red, orange, yellow, green and blue). Tissue types from each individual are color coded with green (normal, NP), orange (premalignant lesions, PIN), blue (primary tumor, TU), and red (lymph node metastasis, LNM). Deletions (marked in blue) and amplifications (red) are shown for chromosomes 1 to X.
- B) Unsupervised hierarchical clustering of intertumoral methylation levels based on the top 1 % most variable CpG sites (n=4457). Blue indicates low and yellow represents high methylation level (from 0 to 1).
- C) Cumulative distribution of methylation specificity for cases 1 to 5. The DNA methylation specificity of a CpG site was defined based on the Jensen-Shannon divergence (Ziller et al., 2013). Aberrations that are found across most tumor sites display low specificity whereas aberrations present only in a subset of tumor regions have high specificity. Orange lines display specificity for all hypermethylated CpG sites for a given case; blue lines show specificity for hypomethylated CpGs.
- D) Cumulative distribution of copy-number specificity for cases 1 to 5. Red lines display specificity for all gained chromosomal regions for a given case; blue lines show specificity for all lost chromosomal regions.
- E) Promoter CpG island hypermethylation (left) and deletion (right) frequency of known cancer (www.genome.jp/kegg/; entry hsa05215) and known prostate cancer (www.genome.jp/kegg/; entry ko05215) driver genes, respectively. Frequency of 1 means a given aberration was found across all tumor regions (excluding normal-like PIN lesions).
- F) Boxplot showing tumor/normal expression levels of genes with both recurrent promoter hypermethylation across all tumor regions and significantly (Benjamini-Hochberg adjusted p-value<0.05) reduced transcription in prostate cancer. Expression data was obtained from (Taylor et al., 2010).
- G) Density estimation of the ratio between methylation levels at ubiquitously (all tumor regions in all five cases, n=47), shared (not in all, but more than one, n=9), or private (only in one, n=10) hypermethylated promoter CpG islands and the estimated tumor purity (material and methods). Values around 1 suggest a hypermethylation event is found in all tumor cells within a given region, while lower numbers indicate subclonality
- H) PTGS2 promoter CpG island methylation for all tumor regions of case 4 normalized by the estimated tumor purity.

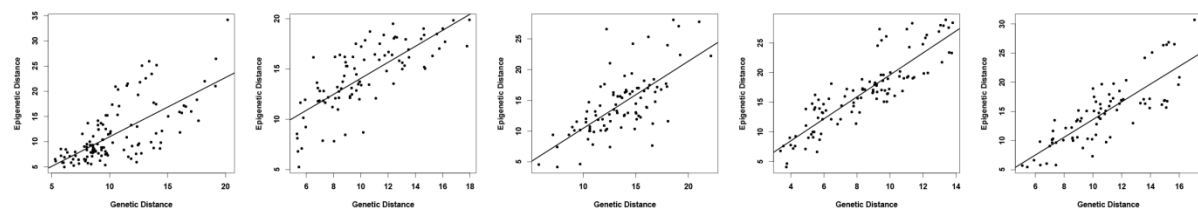
Figure S3

A

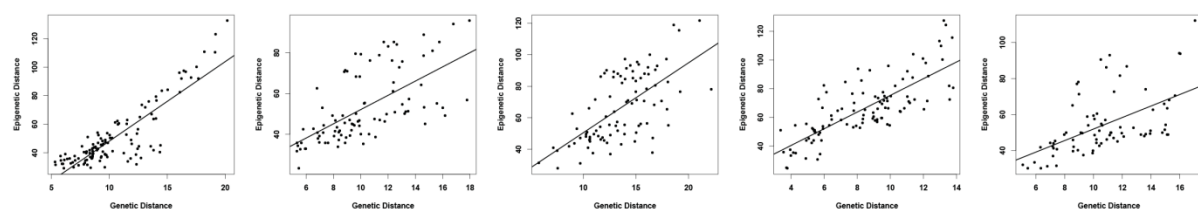
CASE



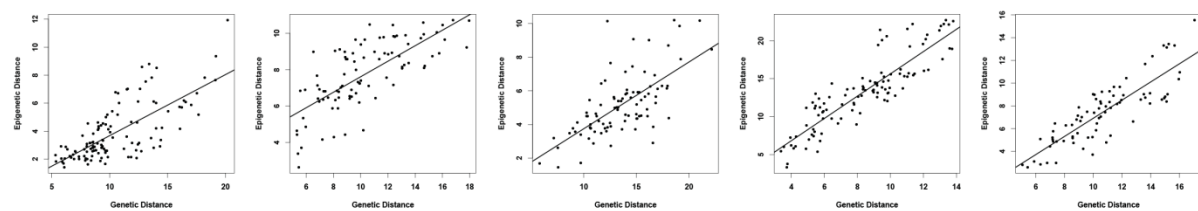
B



C



D



E

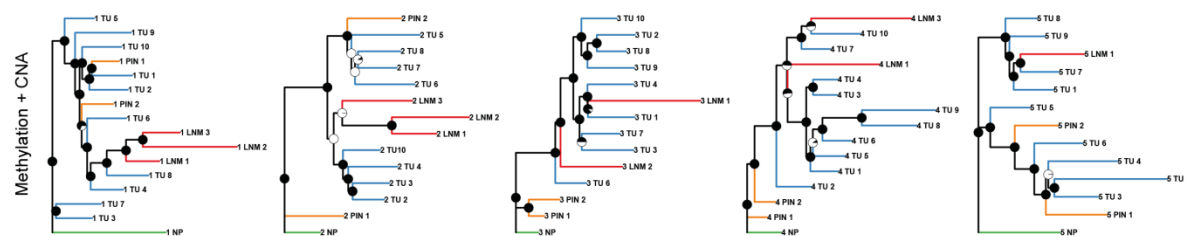
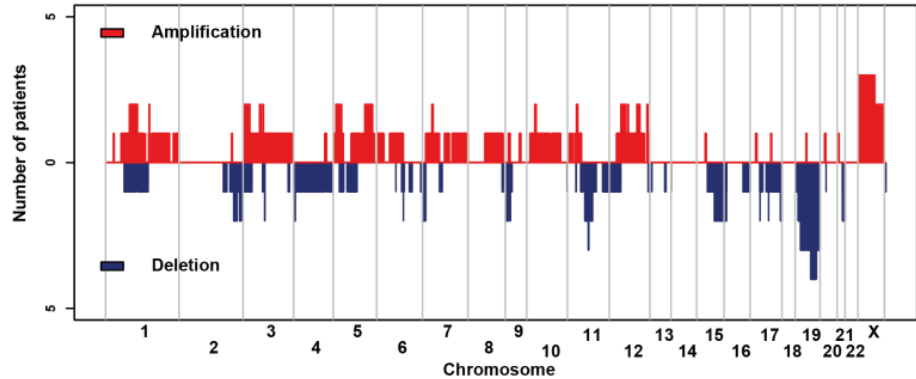


Figure S3, related to Figure 2. Unified evolution of copy-number and DNA methylation patterns.

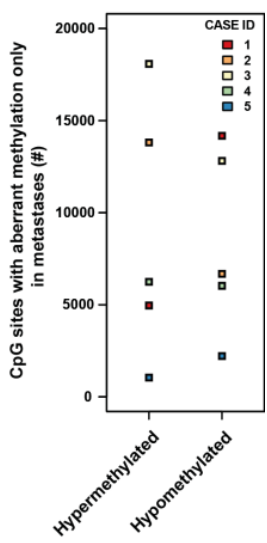
- A) Rooted phylogenies showing the clonal relationships based on copy-number alterations (top panel) or DNA methylation patterns (bottom panel) for cases 1 to 5. Tissue types from each individual are color coded with normal (green), PIN (orange), primary tumor (blue), and lymph node metastasis (red). Pie charts in the proximity of the nodes indicate the proportion (black) of bootstrap trees ($B=1000$ bootstrap replicates) which also resolved the clade at the endpoints of that branch.
- B) Linear relationship between genetic and epigenetic Euclidean distances. Genetic and epigenetic distances were obtained by using the Euclidean distance measure of copy-number and DNA methylation patterns, respectively. X-axes show the values of the copy-number Euclidean distance matrix and Y-axes display Euclidean distances based on DNA methylation patterns for cases 1 to 5. Lines indicate the result of the linear regression analysis.
- C) Linear relationship between copy-number and DNA methylation Euclidean distances based on all analyzed CpG sites ($n=445694$).
- D) Linear relationship after removal of all CpG sites within non-diploid copy-number regions.
- E) Rooted phylogenies showing the clonal relationships based on copy-number alteration and DNA methylation patterns. Pie charts in the proximity of the nodes indicate the proportion (black) of bootstrap trees ($B=1000$ bootstrap replicates) which also resolved the clade at the endpoints of that branch.

Figure S4

A



B



C

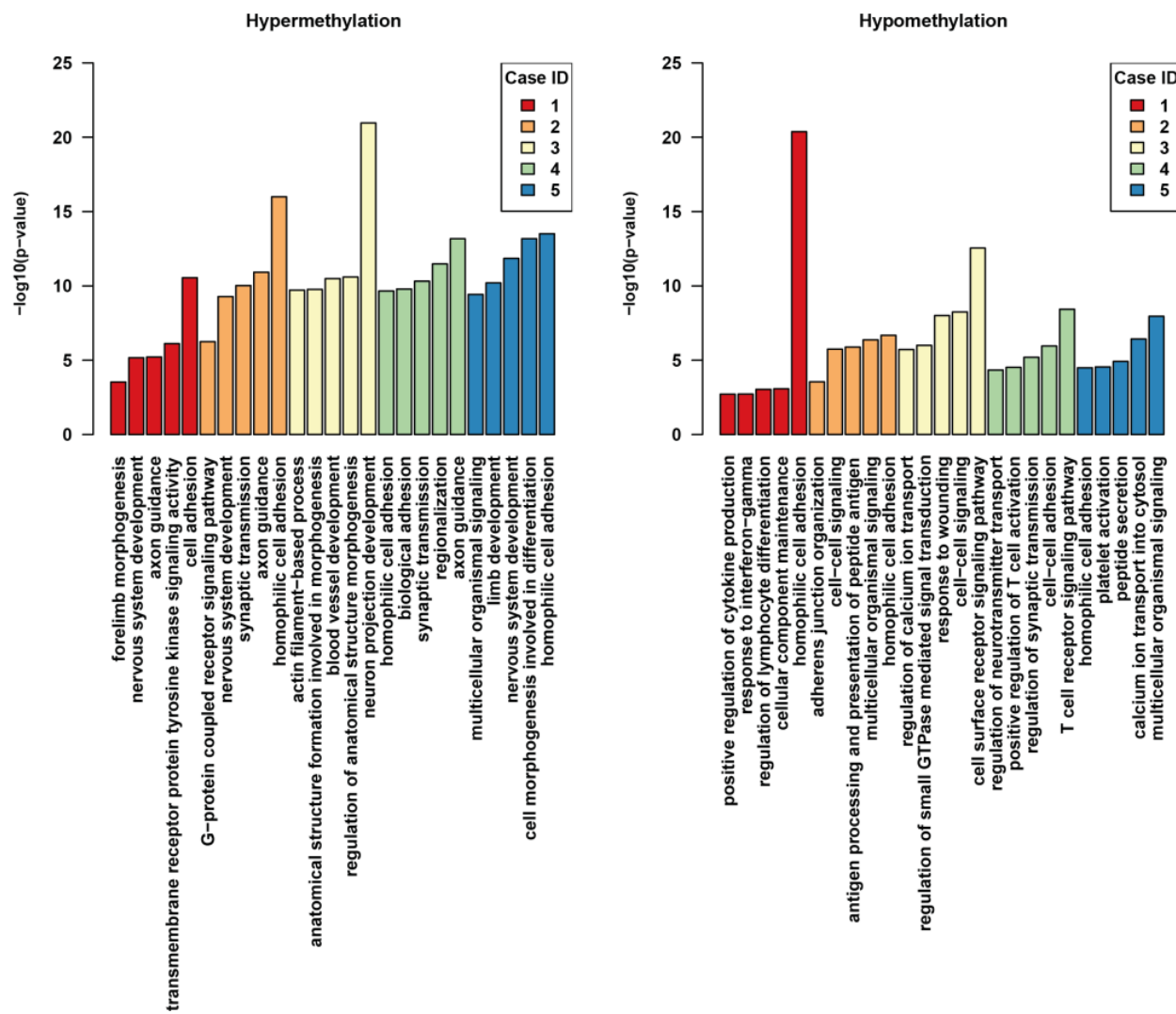


Figure S4, related to Figure 3. Metastasis-specific genetic and epigenetic aberrations.

- A) Metastasis-specific chromosomal deletions (blue) or gains (red). The height of the bar indicates the number of cases a region was specifically found to be deleted or gained in at least one metastasis.
- B) Number of metastasis-specific hyper-/hypomethylation events for each of the 5 cases.
- C) Biological processes that are over-represented by genes carrying at least one metastasis-specific methylation event. Hypergeometric tests for association of Gene Ontology (GO) and genes were performed using the GOstats R packages. Ordered by significance, the 5 most significant terms are shown for each case.

Supplemental Experimental Procedures

Patient Material

Research using pseudomized human left-over tissue samples from routine diagnosis is covered by the Hamburgisches Krankenhausgesetz (HmbKHG) §12. The study protocol (PV3552) was approved by the Institutional Review Board of the Aerztekammer Hamburg (Chair: Prof. T. Weber). Informed consent was obtained from all subjects involved in this study. A total of five prostate cancer patients were selected that had large unifocal prostate cancers, adjacent high grade PIN that was large enough to be separately analyzed, and at least 3 nodal metastases measuring $\geq 1\text{cm}$. All prostates from these patients had been prepared according to standard protocols (Erbersdobler et al., 2002) including complete paraffin embedding of the entire prostates. From each patient, 10 different tumor areas, that were located as far apart from each other as possible were selected for molecular analysis. In addition, 2 different areas of high grade Prostatic Intraepithelial Neoplasia (PIN) and 3 nodal metastases were selected. From each selected tumor and PIN areas as well as from normal prostatic tissue located as far as possible away from the nearest PIN or cancer area, a tissue cylinder measuring 0.6mm in diameter and 4mm in length was taken for DNA extraction. Tumor cellularity was assessed by visual inspection by an experienced pathologist. Only samples were selected, that had a tumor cell content of more than 60%. Tumor cellularity was additionally assessed by the measurement of GSTP1 promoter methylation (based on the Illumina 450K probes; cg06928838, cg09038676, cg22224704, and cg26250609) as a good correlation ($R=0.9$) between GSTP1 promoter methylation and purity estimates based on germline SNV allele frequency in LOH regions for another cohort of prostate cancer samples was observed (**Figure S1A**). Tumor specimens with median GSTP1 methylation below 40% were excluded from the analysis (2_TU_1, 2_TU_9, 3_TU_5, 4_LNM_2, 5_TU_10, 5_LNM_2). Retained specimens ranged in tumor content from 45 % to 70 % which was better or comparable with other studies that had measured tumor cellularity by sequencing based methods(Baca et al., 2013; Su et al., 2012) (**Figure S1B**).

Nucleic Acid Isolation

DNA from Formaldehyde Fixed-Paraffin Embedded (FFPE) samples was isolated using the QIAamp DNA FFPE Tissue Kit (Qiagen, Hilden, Germany) according to the manufacturer's protocols with an additional cleaning step. Briefly, paraffin blocks were heated at 65°C with xylene 3 times for 5mins in the thermomixer (350rpm) to melt paraffin. After washing with 100% ethanol, pellet was resuspended in ATL buffer containing proteinase K and incubated overnight at 56°C. Additional 3-4hours of incubation with proteinase K was performed before DNA isolation. Approximately 250ng of DNA was used for subsequent bisulfite conversion and genome-wide DNA methylation profiling.

DNA Methylation Profiling

Genome-wide DNA methylation was analyzed on Illumina HumanMethylation450 BeadChip arrays (Illumina, San Diego, USA). Methylation of tumor and normal prostate samples was measured according to the manufacturer's instruction at the DKFZ Genomics and Proteomics Core Facility (Heidelberg, Germany). Data are available at the European Genome-Phenome Archive (www.ebi.ac.uk/ega/) and are accessible through EGA Series accession number EGAS00001000682. Methylation values were subset-quantile within array normalized (SWAN) and afterwards filtered according to the following criteria in RnBeads (<http://rnbeads.mpi-inf.mpg.de/>): probes missing information for a single sample or having a detection p-value below 0.01 (n=36662) and probes measuring methylation in a non CpG context (n=3156) were removed. Additionally, probes containing a single-nucleotide polymorphism (dbSNP132 Common) (n=92428) were excluded for any interindividual comparison. No strong batch effects were identified and there was a very high concordance of methylation levels measured by Illumina 450K and reduced representation bisulfite sequencing (RRBS) (**Figure S1**). Hyper-/hypomethylation were arbitrarily defined by at least 20% in-/decrease relative to matched normal prostate epithelium, respectively. Methylation levels (beta values) were used for all subsequent analyses.

Copy-Number Alterations Profiling

CNAs were interrogated from the Illumina HumanMethylation450 BeadChip using the sum of the methylated and unmethylated signal intensities as previously described with modifications (Sturm et al., 2012). Probes found to be highly variable between the five normal prostate epithelia were excluded from the analysis according to the following criteria: Removal of probes not within the 0.05 and 0.85 quantile of median summed values or over the 0.8 quantile of the median absolute deviation. Log2-ratios of specimens to the median value of normal prostate epithelia were calculated, and sample noisiness was determined as the median absolute deviation of adjacent probes. Probes were then combined by joining 20 adjacent probes, and resulting genomic windows less than 100kb in size were iteratively merged with adjacent windows of smaller size. Windows bigger in size than 5Mb were excluded from the analysis, resulting in a total of 9601 windows throughout the genome. For every window, the median probe value was calculated and shifted to minimize the median absolute deviation from all windows to zero for every specimen. For the estimation of copy number variation specificities, Bayesian reversible jump hidden Markov models(Rueda and Diaz-Uriarte, 2007) were fitted to these data, incorporating model uncertainty by Bayesian model averaging, with the possible copy number states deletion, neutral or gain/amplification. The R package RJaCGH v2.0.2 was used for this with the following parameter specifications (default settings for all other parameters): var.equal=FALSE, window=1, TOT=20000, NC=4, maxVar=2 x sample variance. For all other copy number variation analyses, segmentation was performed by applying the circular binary algorithm(Olshen et al., 2004) using the following settings: min.width=10, nperm=32000, alpha=0.001, undo.splits="sdundo", undo.SD=0.5. The median value of windows contained in each segment was calculated, and classified as homozygous (coded in

further analyses as state -2) or hemizygous deletion (-1), neutral (0), gain (+1) or amplification (+2) by the following arbitrary thresholds: -0.5, -0.08, 0.08, 0.3. The posterior probability estimates for deletion and for gain/amplification obtained with RJaCGH were used for copy number variation specificity, while the log₂ ratios were used for all other analyses. Metastasis 3_LNM_3 and 5_LNM_3 were excluded from the analysis due to high noisiness of the profile (**Figure S1E**).

Unsupervised Hierarchical Clustering

Unsupervised hierarchical clustering of SWAN-normalized methylation values from all specimens was performed using a Euclidean distance measure of the 1% (n=4457) most variable CpG sites (by standard deviation) and Ward's linkage. Hierarchical clustering of case-wise intratumoral methylation levels was performed as described in the Experimental Procedures.

Methylation and Copy-Number Alteration Specificity

Patient-level specificities of (i) hypo- and hyper-methylation, (ii) copy number deletion and (iii) copy number gain/amplification were determined as previously described using the Jensen-Shannon divergence (Ziller et al., 2013) of the methylation level distribution (i) or the posterior probability distributions determined by the RJaCGH method (Rueda and Diaz-Uriarte, 2009) for copy number deletion (ii) or gain/amplification (iii) across all samples corresponding to a patient.

Reduced Representation Bisulfite Sequencing

Methylation analysis by reduced representation bisulfite sequencing (RRBS) was performed as previously described (Shipony et al., 2014). CpG sites with coverage of at least 10 were used to compare average methylation between Illumina 450K and RRBS.

Supplemental References

- Baca, S.C., Prandi, D., Lawrence, M.S., Mosquera, J.M., Romanel, A., Drier, Y., Park, K., Kitabayashi, N., MacDonald, T.Y., Ghandi, M., *et al.* (2013). Punctuated evolution of prostate cancer genomes. *Cell* 153, 666-677.
- Erbersdobler, A., Fritz, H., Schnoger, S., Graefen, M., Hammerer, P., Huland, H., and Henke, R.P. (2002). Tumour grade, proliferation, apoptosis, microvessel density, p53, and bcl-2 in prostate cancers: differences between tumours located in the transition zone and in the peripheral zone. *European urology* 41, 40-46.
- Gutierrez-Hartmann, A., Duval, D.L., and Bradford, A.P. (2007). ETS transcription factors in endocrine systems. *Trends in endocrinology and metabolism: TEM* 18, 150-158.
- Olshen, A.B., Venkatraman, E.S., Lucito, R., and Wigler, M. (2004). Circular binary segmentation for the analysis of array-based DNA copy number data. *Biostatistics* 5, 557-572.
- Rueda, O.M., and Diaz-Uriarte, R. (2007). Flexible and accurate detection of genomic copy-number changes from aCGH. *PLoS computational biology* 3, e122.
- Rueda, O.M., and Diaz-Uriarte, R. (2009). RJaCGH: Bayesian analysis of aCGH arrays for detecting copy number changes and recurrent regions. *Bioinformatics* 25, 1959-1960.
- Shipony, Z., Mukamel, Z., Mendelson Cohen, N., Landan, G., Chomsky E., Reich Zeliger, S., Chagit Fried, Y., Ainbinder , E., Friedman, N., Tanay, A. (2014). Dynamic and stable maintenance of epigenetic memory in pluripotent and somatic cells. *Nature*, accepted.
- Sturm, D., Witt, H., Hovestadt, V., Khuong-Quang, D.A., Jones, D.T., Konermann, C., Pfaff, E., Tonjes, M., Sill, M., Bender, S., *et al.* (2012). Hotspot Mutations in H3F3A and IDH1 Define Distinct Epigenetic and Biological Subgroups of Glioblastoma. *Cancer cell* 22, 425-437.
- Su, X., Zhang, L., Zhang, J., Meric-Bernstam, F., and Weinstein, J.N. (2012). PurityEst: estimating purity of human tumor samples using next-generation sequencing data. *Bioinformatics* 28, 2265-2266.
- Taylor, B.S., Schultz, N., Hieronymus, H., Gopalan, A., Xiao, Y., Carver, B.S., Arora, V.K., Kaushik, P., Cerami, E., Reva, B., *et al.* (2010). Integrative genomic profiling of human prostate cancer. *Cancer cell* 18, 11-22.
- Ziller, M.J., Gu, H., Muller, F., Donaghey, J., Tsai, L.T., Kohlbacher, O., De Jager, P.L., Rosen, E.D., Bennett, D.A., Bernstein, B.E., *et al.* (2013). Charting a dynamic DNA methylation landscape of the human genome. *Nature*.